International Journal of Nanomedicine

Dovepress
open access to scientific and medical research

Open Access Full Text Article

ORIGINAL RESEARCH

Composite iron oxide–Prussian blue nanoparticles for magnetically guided T_1-weighted magnetic resonance imaging and photothermal therapy of tumors

This article was published in the following Dove Press journal:
International Journal of Nanomedicine
5 September 2017
Number of times this article has been viewed

Shraddha S Kale[1,2]
Rachel A Burga[1,3]
Elizabeth E Sweeney[1]
Zungho Zun[4–6]
Raymond W Sze[1,4–6]
Anthony Tuesca[7]
J Anand Subramony[7]
Rohan Fernandes[1,3,5,6]

[1]The Sheikh Zayed Institute for Pediatric Surgical Innovation, Children's National Health System, Washington, DC, USA; [2]Department of Biomedical Engineering, George Washington University, Washington, DC, USA; [3]The Institute for Biomedical Sciences, George Washington University, Washington, DC, USA; [4]Division of Diagnostic Imaging and Radiology, Children's National Health System, Washington, DC, USA; [5]Department of Radiology, George Washington University, Washington, DC, USA; [6]Department of Pediatrics, George Washington University, Washington, DC, USA; [7]MedImmune LLC, Gaithersburg, MD, USA

Correspondence: Rohan Fernandes
The Sheikh Zayed Institute for Pediatric Surgical Innovation, Children's National Health System, 111 Michigan Ave NW, Washington, DC 20010, USA
Tel +1 202 476 5290
Email rfernand@childensnational.org

Abstract: Theranostic nanoparticles offer the potential for mixing and matching disparate diagnostic and therapeutic functionalities within a single nanoparticle for the personalized treatment of diseases. In this article, we present composite iron oxide-gadolinium-containing Prussian blue nanoparticles (Fe_3O_4@GdPB) as a novel theranostic agent for T_1-weighted magnetic resonance imaging (MRI) and photothermal therapy (PTT) of tumors. These particles combine the well-described properties and safety profiles of the constituent Fe_3O_4 nanoparticles and gadolinium-containing Prussian blue nanoparticles. The Fe_3O_4@GdPB nanoparticles function both as effective MRI contrast agents and PTT agents as determined by characterizing studies performed in vitro and retain their properties in the presence of cells. Importantly, the Fe_3O_4@GdPB nanoparticles function as effective MRI contrast agents in vivo by increasing signal:noise ratios in T_1-weighted scans of tumors and as effective PTT agents in vivo by decreasing tumor growth rates and increasing survival in an animal model of neuroblastoma. These findings demonstrate the potential of the Fe_3O_4@GdPB nanoparticles to function as effective theranostic agents.

Keywords: theranostics, Prussian blue, iron oxide, MRI, photothermal therapy, cancer

Introduction

Theranostics refers to the use of a diagnostic agent (Dx) in tandem with a therapeutic agent (Rx) for the personalized treatment of diseases.[1] A well-known example of a commercialized theranostic is the use of HercepTest® (Agilent, Santa Clara, CA, USA) in combination with Herceptin® (Genentech, South San Francisco, CA, USA) for treating breast cancer.[2] However, this approach requires the sequential administration of the paired Dx/Rx agents. A more desirable and potentially straightforward approach would be the simultaneous administration of the Dx/Rx agents to shorten procedure times while potentially improving patient comfort. Within this context, advances in the field of nanotechnology over the past few decades have facilitated the synthesis of nanoparticles with diverse and complementary diagnostic and therapeutic properties that can be incorporated within a single theranostic nanoparticle.[3,4] These include iron oxide nanoparticles,[5,6] carbon nanotubes,[7,8] gold nanorods,[9,10] dendrimers,[11,12] and vesicles,[13,14] of which multiple nanoparticles are already in the clinic.[15,16] A key design criterion in the synthesis of theranostic nanoparticles, in addition to their complementary Dx/Rx properties, is that the component materials of the nanoparticles are biocompatible

submit your manuscript | www.dovepress.com
Dovepress
http://dx.doi.org/10.2147/IJN.S144515

and/or safe for human use. Therefore, a compelling starting point would be to synthesize theranostic nanoparticles composed of materials with a known safety profile.

To this end, in this study, we describe the design, synthesis, and utilization of composite iron oxide-gadolinium-containing Prussian blue nanoparticles (Fe_3O_4@GdPB) as theranostic agents. Our Fe_3O_4@GdPB contain the following: Fe_3O_4, a US Food and Drug Administration (FDA)-approved material that has been used for T_2-weighted (T2W) magnetic resonance imaging (MRI, in Combidex);[16,17] Prussian blue, an FDA-approved material used in radiation poisoning treatment (as Radiogardase);[18–20] and gadolinium, a key component of clinical MRI contrast agents including Magnevist and Gadovist.[21,22] Earlier reports have described the synthesis of magnetic Prussian blue nanoparticles (without gadolinium) for T2W imaging combined with photothermal therapy (PTT) of tumors and gene transfection or chemotherapy combined with PTT of tumors.[23–25]

Building on these earlier findings, we utilize our Fe_3O_4@GdPB nanoparticles for magnetically guided, T_1-weighted (T1W) imaging and PTT of tumors. Compared with T2W images, T1W images offer several advantages including enhanced visualization of vascular structures, key for the entry of Dx and Rx agents into tumors, and are less prone to artifacts such as those present in fluid-filled structures in particular.[26] Under external magnetic guidance, T1W images offer the potential to visualize the entry of the composite Dx/Rx agents into a tumor through its vasculature in real-time, allowing for a more precise administration of PTT to targeted tumors. This approach can facilitate improved tumor treatment margins, which has implications not only for local tumor control but also in prevention of its recurrence.

In seeking to leverage these aforementioned advantages, we describe the synthesis and characterization of composite Fe_3O_4@GdPB nanoparticles. We determine the MRI and photothermal properties of the nanoparticles. Finally, as a proof-of-principle, we utilize the Fe_3O_4@GdPB nanoparticles for T1W MRI and PTT in an animal model of neuroblastoma,[27,28] a prevalent solid tumor of childhood and a leading cause of cancer-related death in children.[29,30] The findings of our study are crucial for further developing our composite theranostic nanoparticles for magnetically targeted, image-guided photothermal destruction of tumors.

Materials and methods

Materials

Ultrapure water used in this study was obtained from a Milli-Q® system (MilliporeSigma; resistivity ≥17.8 MΩ cm). All chemicals were purchased from Sigma-Aldrich, and biological reagents were purchased from Thermo Fisher Scientific and used as supplied without further purification unless noted otherwise.

Synthesis of Fe_3O_4@GdPB nanoparticles

Fe_3O_4@GdPB nanoparticles were synthesized using a scheme modified from previously described studies.[23–25] Briefly, coprecipitation was used to synthesize Fe_3O_4 nanoparticles where a 1:2 molar ratio of Fe^{2+}:Fe^{3+} was added dropwise into a stirred solution of 1 M NaOH.[31] The resultant black precipitate containing Fe_3O_4 nanoparticles was thoroughly rinsed and dispersed in ultrapure water by centrifugation (at least three times at 22,000× *g* for 10 minutes) and resuspension (using sonication to disperse the pellet, as needed). Next, Fe_3O_4 nanoparticles (diluted to 1 mg/mL) were added dropwise into a solution of $K_4[Fe(CN)_6]$ (2 mM; pH =3) in a sonicator bath with continuous stirring maintained at 50°C. The above-mentioned solution was then added to a solution containing $Gd(NO_3)_3$ and $FeCl_3$ (2 mM; pH =3) under the sonication, stirring, and heating conditions described earlier. Finally, the resultant solution containing Fe_3O_4@GdPb nanoparticles was rinsed and dispersed in ultrapure water as described earlier.

Characterization of the Fe_3O_4@GdPB nanoparticles

The size (hydrodynamic diameter) and charge (zeta potential) distributions of the Fe_3O_4@GdPB nanoparticles were compared with both Fe_3O_4 and GdPB nanoparticles (previously synthesized by us)[32,33] using dynamic light scattering on a Zetasizer Nano ZS (Malvern Instruments, Malvern, UK). Multiday stability of the Fe_3O_4@GdPB nanoparticles in ultrapure water was assessed by measuring their hydrodynamic size distributions every 24 hours over 5 days using dynamic light scattering. The visible-near infrared (NIR) spectra of 1 mg/mL suspensions of the three different types of nanoparticles in ultrapure water were measured using a Genesys 10S Ultraviolet-Visible (UV-Vis) spectrophotometer (Thermo Fisher Scientific, Waltham, MA, USA). Transmission electron microscopy (TEM) images of the Fe_3O_4 and Fe_3O_4@GdPB nanoparticles were obtained by loading 5 µL of the nanoparticle suspensions separately onto copper grids (Electron Microscopy Sciences, Hatfield, PA, USA) using a JEOL JEM 2100 field-emission gun scanning transmission electron microscope (TEM; JEOL, Peabody, MA, USA). Analysis of the size distributions of the nanoparticles was performed using ImageJ (National Institutes of Health). Energy-dispersive X-ray spectroscopy (EDS) was performed using an INCA 250 analysis system (Oxford Instruments, Abingdon, UK) coupled to the TEM. A total of seven scans were performed

on different parts of the grid and then averaged to obtain the relative percentages of Gd, Fe, and K.

MRI properties of the Fe_3O_4@GdPB nanoparticles

The MR relaxivities of the Fe_3O_4@GdPB nanoparticles were measured using a clinical horizontal 3 T magnet (GE Healthcare, Chicago, IL, USA). Phantoms containing varying concentrations of the nanoparticles (Fe_3O_4, GdPB, and Fe_3O_4@GdPB) were prepared in 96-well plates in 0.5% agarose solutions. A constant temperature of 23°C was maintained for all the measurements. The phantoms were placed on a 2% solid block of agar and secured by tape at the center of an 8-channel high definition brain coil.[32,34] T_1 and T_2 relaxation times were measured in the same coronal 0.5 mm thick slice. Inversion times (TI) were varied (from 50 to 4,000 ms) to obtain T_1 measurements, while echo times (TE) were varied (from 12 to 245 ms) to obtain T_2 measurements. Image processing software, OsiriX, was used to analyze the signal intensity within a region of interest (ROI) of the acquired images. To measure the T_1 inversion, the signal intensity was plotted against the TI values, while signal intensity was plotted against TE values for the T_2 decay curves. The data were then fitted using the following equations:

$$T_1 : SI = A - Be^{\left(\frac{-T_I}{T_1}\right)}$$

$$T_2 : SI = Ce^{\left(\frac{-T_E}{T_2}\right)}$$

where SI is the signal intensity within the ROI, and A, B, and C are positive constants. The R_1 and R_2 relaxation rates were then obtained by calculating $1/T_1$ and $1/T_2$, respectively. The relaxation rates obtained were plotted against the concentrations of the corresponding contrast agent (Gd for T1W images and Fe for T2W images) and slopes of these plots yielded the relaxivities of the nanoparticles.

Photothermal properties of the Fe_3O_4@GdPB nanoparticles

The photothermal properties of the Fe_3O_4@GdPB nanoparticles were measured using aqueous dispersions of the nanoparticles irradiated using an 808 nm NIR laser (Laserglow Technologies, Toronto, Canada), as previously described.[35] The PTT capabilities of the Fe_3O_4@GdPB nanoparticles were measured as a function of concentration by varying the concentration of the nanoparticles from 0.01 to 0.2 mg/mL at a fixed laser fluence (power density) of 1.875 W/cm^2 for 10 minutes. The PTT capabilities were measured as a function of varying laser fluence (0.625–3.125 W/cm^2) by irradiating 0.1 mg/mL Fe_3O_4@GdPB for 10 minutes. The stability of the nanoparticles as a photothermal agent was assessed by a cyclic heating/cooling study where 1 mg/mL Fe_3O_4@GdPB was irradiated by the NIR laser (laser on/off times =10 minutes each). The photothermal conversion efficiency of the Fe_3O_4@GdPB nanoparticles was measured by first heating 0.1 mg/mL of the nanoparticles with the NIR laser at a fluence of 1.875 W/cm^2 for 10 minutes. The laser was then turned off, and the cooling kinetics of the nanoparticles was measured as a function of time. The photothermal conversion efficiency was calculated using the following equation described by Roper et al.[36]

$$\eta_T = \frac{hA\,(T_{max} - T_{amb}) - Q_0}{I\,(1 - 10^{-A_\lambda})}$$

Where h is the heat transfer coefficient, A is the surface area of heat transfer of the system, T_{max} is the maximum system temperature, T_{amb} is the ambient temperature, Q_0 is the rate of heat input due to absorption of light energy by water, I is the incident laser power, and A_λ is the absorbance of the Fe_3O_4@GdPB at 808 nm.

Intrinsic and PTT-induced cytotoxicity of the Fe_3O_4@GdPB nanoparticles

The intrinsic and PTT-induced cytotoxicity of the Fe_3O_4@GdPB nanoparticles in vitro was measured using the murine neuroblastoma cell line Neuro2a (ATCC). Briefly, Neuro2a was seeded in 96-well plates and incubated with either vehicle or varying concentrations of the Fe_3O_4@GdPB nanoparticles (0.01–0.5 mg/mL) with or without laser irradiation using the NIR laser (1.5 W/cm^2; 10 minutes). Twenty-four hours after the treatment, cell viability was assessed using the CellTiter-Glo luminescent cell viability assay (Promega Corporation, Madison, WI, USA). Each treatment was conducted with at least three replicates.

Animals

All animal studies were conducted in accordance with protocols approved by the Institutional Animal Care and Use Committee (IACUC) at Children's National Health System and were conducted to ensure humane care of the animals as per the IACUC's guidelines. For the animal studies, 4–6-week old female A/J mice were purchased from Jackson Laboratory, and the animals were acclimated for 3–4 days prior to commencing the studies.

Animal studies

To establish the murine neuroblastoma model, one million Neuro2a cells suspended in phosphate-buffered saline were

injected subcutaneously into the shaved backs of 4–6-week old female A/J mice. Tumor growth was monitored by routine caliper measurements, as previously described.[35,37] All treatments commenced only after the Neuro2a tumors reached a diameter of at least 5 mm (~60 mm^3). Tumor-bearing mice were divided into three groups (n≥9 mice/group): 1) untreated group: receiving no further treatment, 2) Fe_3O_4@GdPB group: receiving 100 µL of 1 mg/mL Fe_3O_4@GdPB by tail vein injection, and 3) Fe_3O_4@GdPB + magnet group: receiving 100 µL of 1 mg/mL Fe_3O_4@GdPB by tail vein injection followed by application of an external magnetic field for 10 minutes; by externally affixing a 3,000 Gauss magnet (0.25″×0.25″×0.25″ Nickel-plated neodymium; K&J Magnetics Inc, Pipersville, PA, USA) to the surface of the tumors for mice in this group. After this step, the mice in each group were divided into two cohorts (n≥4 mice/cohort). Mice in cohort 1 were used for MRI. These mice were immediately euthanized after the aforementioned procedures and their tumors extracted. Tumor phantoms were prepared using 5% agarose solutions and T1W images of these tumors were acquired and analyzed as described earlier. Mice in cohort 2 were used for PTT. These mice were irradiated after completing application of the external magnet with the NIR laser (1.5 W/cm^2; 15 minutes). The tumor surface temperature achieved during the laser treatment step was measured using an i7 thermal camera (FLIR, Wilsonville, OR, USA). Post-PTT, tumor growth, and animal survival were monitored.

Statistical analysis

Statistically significant differences between groups were determined by using a Student's *t*-test. The log-rank test was used to determine statistically significant differences in survival, analyzed by generating Kaplan–Meier plots. A *P*-value of <0.05 was considered statistically significant in all studies (denoted by *).

Results and discussion

Synthesis scheme yields Fe_3O_4@GdPB nanoparticles with stable, monodisperse size distributions, and composite properties

The Fe_3O_4@GdPB nanoparticles were synthesized by growing a "shell" of gadolinium-containing Prussian blue on an iron oxide nanoparticle "core" by modifying previously published schemes for synthesizing magnetic Prussian blue nanoparticles (without gadolinium).[23–25] This synthesis relies on the attachment of $Fe(CN_6)^{4-}$ onto the surface of iron oxide nanoparticles at an acidic pH (refer "Materials and methods" section for details), and the subsequent growth of a GdPB shell by the reaction of $Fe(CN_6)^{4-}$, Fe^{3+}, and Gd^{3+} on the surface of the iron oxide nanoparticles. To determine the properties of the Fe_3O_4@GdPB nanoparticles synthesized using the presented two-step scheme (Figure 1A), we first measured the size distributions and charges of the nanoparticles using dynamic light scattering. The synthesis yielded monodisperse Fe_3O_4@GdPB nanoparticles (polydispersity index ~0.2) with a mean hydrodynamic diameter of 164.2 nm, which was higher than the mean hydrodynamic diameters of the constituent Fe_3O_4 (68 nm) and GdPB (91 nm) nanoparticles (Figure 1B). Zeta potential measurements revealed that the Fe_3O_4@GdPB nanoparticles exhibited charges (−16.5 mV) intermediate to those of the constituent Fe_3O_4 (−13.3 mV) and GdPB (−24.8 mV) nanoparticles (Figure 1C). Multiday stability studies using dynamic light scattering demonstrated that aqueous suspensions of the Fe_3O_4@GdPB nanoparticles retained nearly constant size distributions over 5 days (Figure 1D). Visible-NIR spectroscopy of equal concentrations (1 mg/mL each) of Fe_3O_4, GdPB, and Fe_3O_4@GdPB nanoparticles demonstrated that Fe_3O_4@GdPB retained the characteristic absorption band of Prussian blue-based nanoparticles (GdPB) in the 600–900 nm range and, as expected, demonstrated an attenuated absorption band relative to GdPB (Figure 1E). TEM images illustrated individual Fe_3O_4@GdPB nanoparticles (Figure 2A) with a size range of 28.2±8.3 nm, representing an increase in size from the Fe_3O_4 core nanoparticles (without GdPB) that had a size range of 8.0±2.2 nm (Figure S1). EDS scans conducted on seven different areas of the TEM grid revealed that the analyzed nanoparticles comprised both Fe and Gd (Figure 2B). Taken together, these findings demonstrate that our synthesis scheme results in stable Fe_3O_4@GdPB nanoparticles with properties that are a composite of the constituent Fe_3O_4 and GdPB nanoparticles.

Fe_3O_4@GdPB nanoparticles function as effective MRI contrast agents

To determine if the Fe_3O_4@GdPB nanoparticles function as effective MRI contrast agents, we conducted scans of phantoms containing serial dilutions of Fe_3O_4@GdPB and the constituent Fe_3O_4 and GdPB nanoparticles in a clinical 3 T MRI magnet. T1W scans demonstrated that the Fe_3O_4@GdPB nanoparticles generated increased contrast in a concentration-dependent manner (Figure 3A), ie, increased brightening at increased concentrations, similar to GdPB nanoparticles (previously characterized by us and

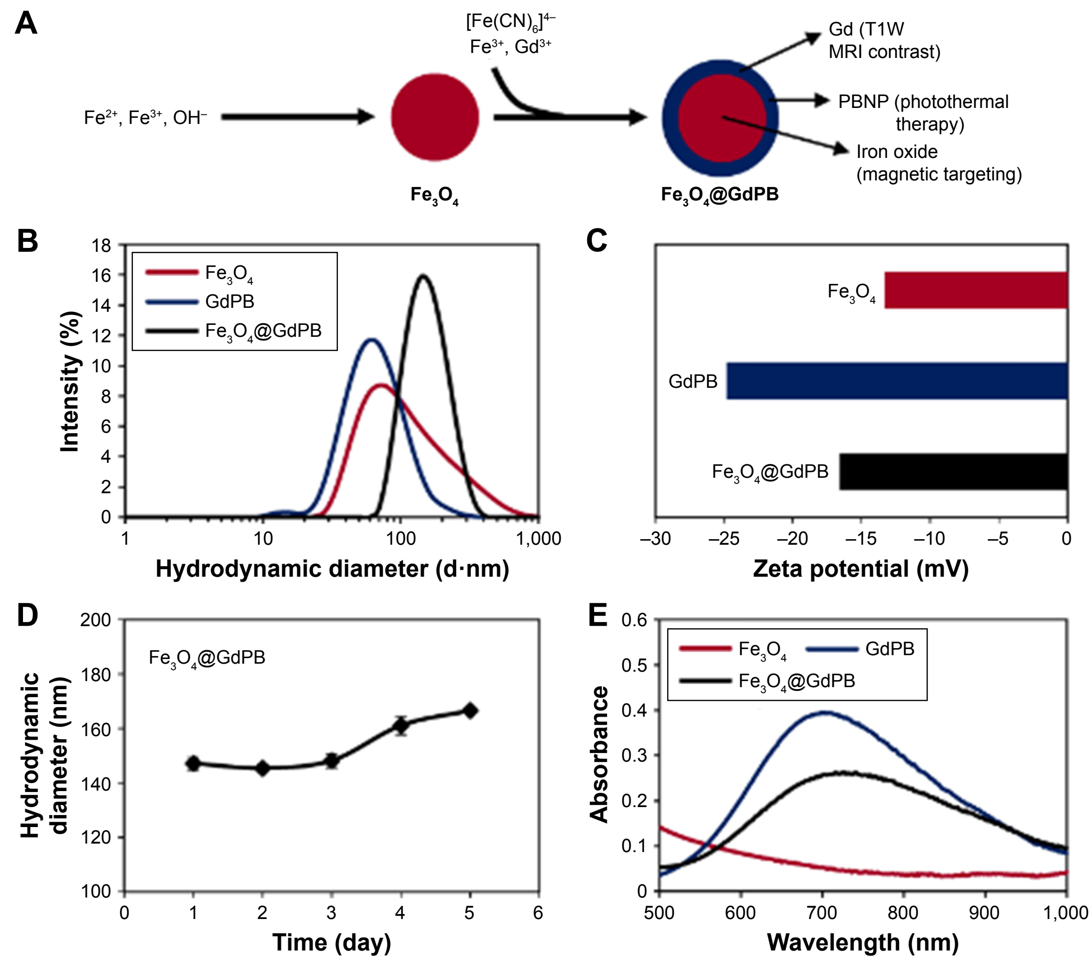

Figure 1 Synthesis and characterization of Fe_3O_4@GdPB nanoparticles.

Notes: (**A**) The two-step scheme employed for synthesizing Fe_3O_4@GdPB nanoparticles. (**B**) Dynamic light scattering-based analysis of the size distributions (hydrodynamic diameters) of Fe_3O_4, GdPB, and Fe_3O_4@GdPB nanoparticles. (**C**) Zeta potentials of Fe_3O_4, GdPB, and Fe_3O_4@GdPB nanoparticles. (**D**) Multiday mean sizes (hydrodynamic diameters) of Fe_3O_4@GdPB nanoparticles measured by dynamic light scattering. (**E**) Visible-near infrared spectra of 1 mg/mL each of Fe_3O_4, GdPB, and Fe_3O_4@GdPB nanoparticles.

Abbreviations: Fe_3O_4@GdPB, composite iron oxide-gadolinium-containing Prussian blue; Fe_3O_4, iron oxide; GdPB, gadolinium-containing Prussian blue; MRI, magnetic resonance imaging; PBNP, Prussian blue nanoparticle; T1W, T_1-weighted.

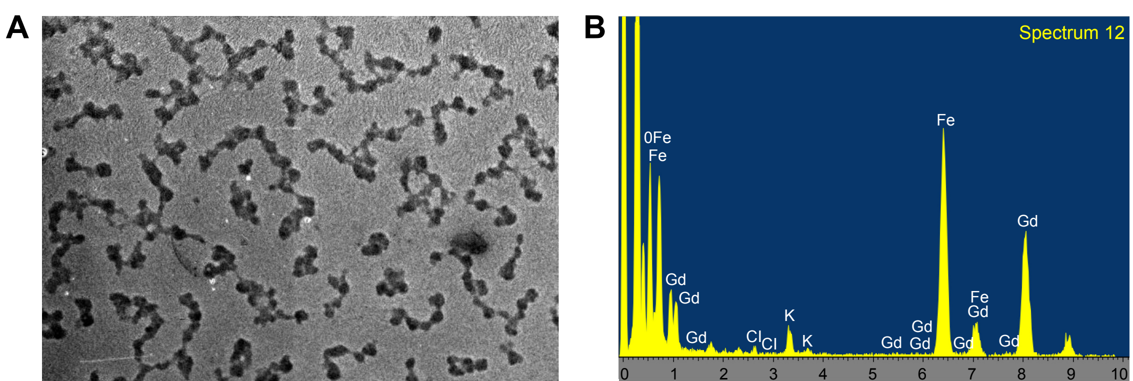

Element	Weight (%)	Atomic (%)
Fe	16.13	5.76
Gd	7.33	0.925

Figure 2 Shape and composition of Fe_3O_4@GdPB NPs.

Notes: (**A**) Transmission electron microscopy image of Fe_3O_4@GdPB NPs. (**B**) Representative energy-dispersive X-ray spectrum of Fe_3O_4@GdPB NPs. The composition was derived by built-in software from the attribution of the electronic energy profile for Fe, K, and Gd.

Abbreviation: Fe_3O_4@GdPB NPs, composite iron oxide-gadolinium-containing Prussian blue nanoparticles.

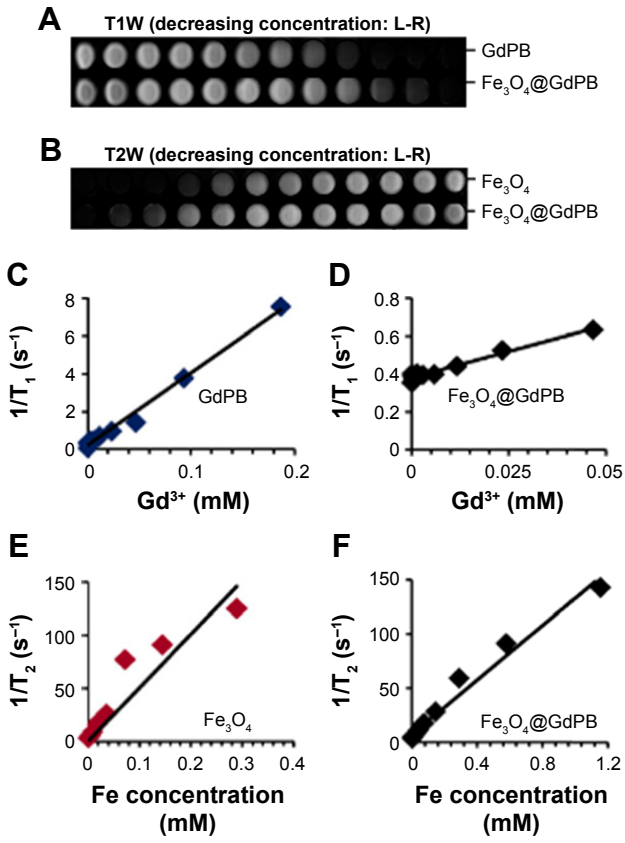

G

Nanoparticle	r_1 (mM^{-1} s^{-1})	r_2 (mM^{-1} s^{-1})
Fe_3O_4	nd	504.7
GdPB	38.4	nd
Fe_3O_4@GdPB	5.5	126.0

Figure 3 MRI properties of Fe_3O_4@GdPB nanoparticles.
Notes: (**A**) T1W MR images of GdPB and Fe_3O_4@GdPB nanoparticles. (**B**) T2W MR images of Fe_3O_4 and Fe_3O_4@GdPB nanoparticles. (**C**–**D**) T_1-relaxation rate ($1/T_1$), as a function of Gd^{3+} concentration (mM) in (**C**) GdPB and (**D**) Fe_3O_4@GdPB nanoparticles. (**E**–**F**) T_2-relaxation rate ($1/T_2$) as a function of Fe concentration (mM) in (**E**) Fe_3O_4 and (**F**) Fe_3O_4@GdPB nanoparticles. (**G**) Relaxivities of Fe_3O_4, GdPB, and Fe_3O_4@GdPB nanoparticles.
Abbreviations: Fe_3O_4@GdPB, composite iron oxide-gadolinium-containing Prussian blue; Fe_3O_4, iron oxide; GdPB, gadolinium-containing Prussian blue; L-R, left-to-right; MRI, magnetic resonance imaging; T1W, T_1-weighted; T2W, T_2-weighted; nd, not determined for this study.

others).[32,38,39] Similarly, T2W scans demonstrated that the Fe_3O_4@GdPB nanoparticles generated increased contrast in a concentration-dependent manner (Figure 3B), ie, increased darkening with increasing concentrations, similar to Fe_3O_4 nanoparticles, which have been well-described in the literature.[5,6] Based on image processing of multiple T1W and T2W scans, we generated relaxation time plots as a function of the contrast agent, namely Gd^{3+} ions for GdPB (Figure 3C) and Fe_3O_4@GdPB (Figure 3D), and Fe for Fe_3O_4 (Figure 3E) and Fe_3O_4@GdPB (Figure 3F). These studies yielded the r_1 and r_2 relaxivities (Figure 3G) of the Fe_3O_4@GdPB nanoparticles: r_1 =5.5 mM^{-1} s^{-1} and r_2 = 126 mM^{-1} s^{-1}. Although the r_1 value of Fe_3O_4@GdPB is lower than that of GdPB (38.4 mM^{-1} s^{-1}), it is in a range similar to most clinically approved, gadolinium-based T_1 contrast agents at a field strength of 3 T, including Magnevist (3.1 mM^{-1} s^{-1}), ProHance (2.8 mM^{-1} s^{-1}), and Omniscan (3.2 mM^{-1} s^{-1}).[22] Additionally, a unique feature to our Fe_3O_4@GdPB is that they can be guided to a particular anatomical location by an external magnetic field, which cannot be achieved using GdPB nanoparticles that have to rely on vasculature for anatomical targeting. If improved contrast in T1W images is desired, the synthesis of Fe_3O_4@GdPB can be appropriately modified to incorporate a larger shell of GdPB with increased loading of Gd^{3+} ions during synthesis over a smaller core of Fe_3O_4. These results suggest that Fe_3O_4@GdPB can function as an effective MRI contrast agent in T1W scans. In parallel with these studies, we analyzed the T_2 relaxivities of Fe_3O_4@GdPB nanoparticles and obtained an r_2 value of 126 mM^{-1} s^{-1} at a 3 T field strength. Although we do not explicitly utilize the T_2 contrast of our Fe_3O_4@GdPB nanoparticles in this study, since the proposed use of our nanoparticles is for PTT of tumors and we have previously discussed the limitations of using T2W images especially for fluid-filled structures, our results demonstrate that there may be future potential of these agents as contrast agents in T2W imaging applications.

Fe_3O_4@GdPB nanoparticles function as effective PTT agents

To quantify the photothermal heating properties of Fe_3O_4@GdPB nanoparticles, we measured their heating as a function of concentration, laser fluence, and multiple cycles of heating and cooling. At a constant laser fluence of 1.875 W/cm^2, the nanoparticles were observed to heat to significantly higher temperatures over the background (water; Figure 4A) with changes in temperature approaching 20°C at a nanoparticle concentration of 0.01 mg/mL and ~35°C at nanoparticle concentrations ≥0.05 mg/mL. At a constant nanoparticle concentration of 1 mg/mL, Fe_3O_4@GdPB was observed to heat to higher temperatures in a laser fluence-dependent manner (Figure 4B). Additionally, the nanoparticles retained their photothermal heating properties over four cycles of heating and cooling (Figure 4C) indicating their stability as photothermal agents over multiple heating cycles. Finally, studies conducted to calculate the photothermal conversion efficiency (Figure 4D) demonstrated that the nanoparticles had a photothermal conversion efficiency of 16.1%, which is consistent with the previously determined photothermal conversion efficiency of Prussian blue nanoparticles (around 20%)[35] despite

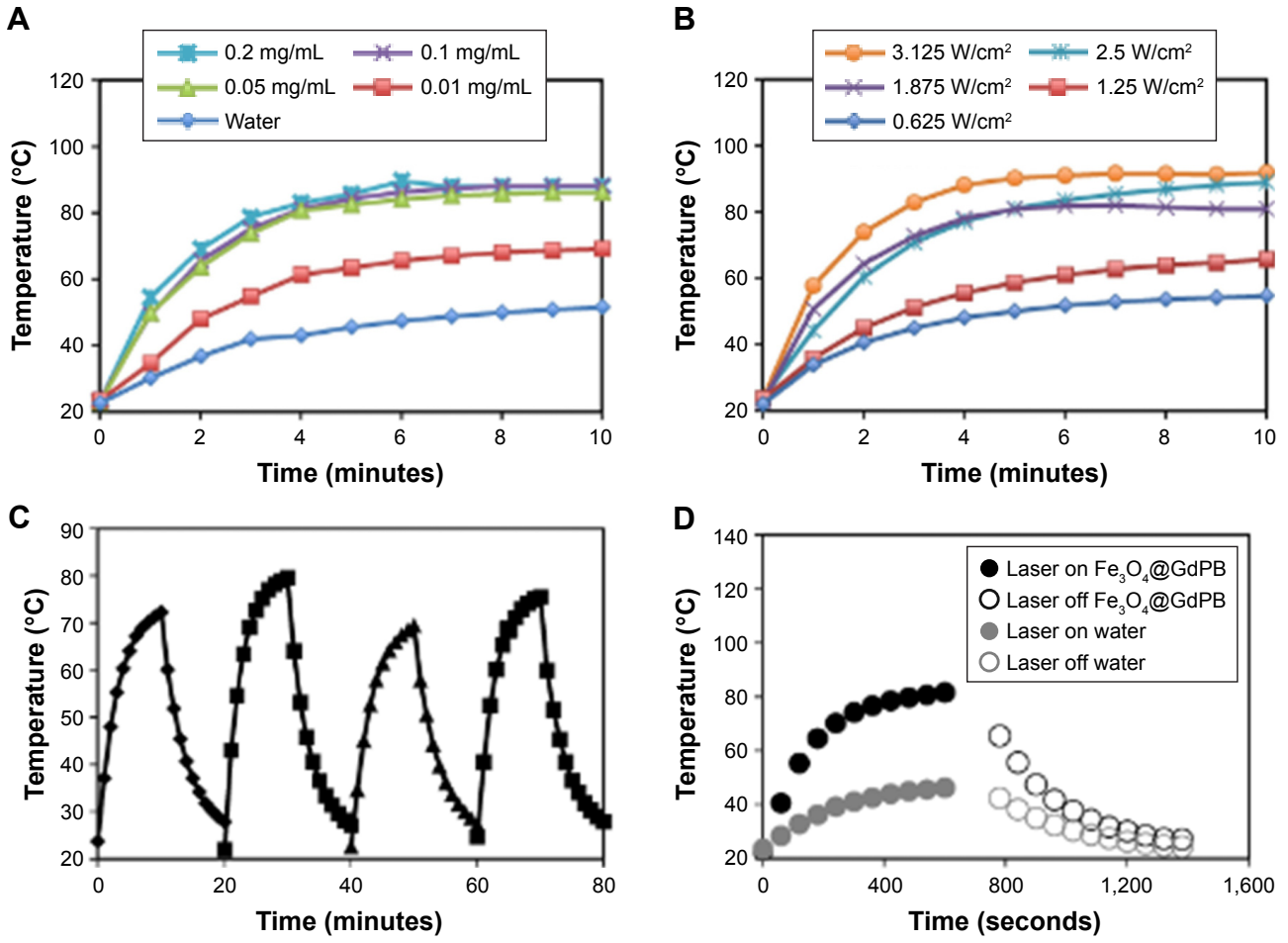

Figure 4 Photothermal heating properties of Fe_3O_4@GdPB nanoparticles.
Notes: (**A**) Photothermal heating of varying concentrations of Fe_3O_4@GdPB nanoparticles at a constant laser fluence of 1.875 W/cm^2 for 10 minutes. (**B**) Photothermal heating of 1 mg/mL Fe_3O_4@GdPB nanoparticles as a function of varying 808 nm NIR laser fluence for 10 minutes. (**C**) Temperature profiles during cyclic heating of 1 mg/mL Fe_3O_4@GdPB nanoparticles using an 808 nm NIR laser (laser on/off time: 10 minutes each). (**D**) Generation of heating and cooling curves of Fe_3O_4@GdPB nanoparticles to calculate their photothermal conversion efficiency.
Abbreviations: Fe_3O_4@GdPB, composite iron oxide-gadolinium-containing Prussian blue; NIR, near infrared.

the fact that Fe_3O_4@GdPB nanoparticles are a composite of both Fe_3O_4 and GdPB. These results demonstrate that Fe_3O_4@GdPB nanoparticles are stable and effective PTT agents.

Fe_3O_4@GdPB nanoparticles are cytotoxic to targeted cells upon photothermal heating

To assess the intrinsic cytotoxicity of our Fe_3O_4@GdPB nanoparticles as well as test whether they can function as effective PTT agents in the presence of cells, we added varying concentrations (0.01–0.5 mg/mL) of the nanoparticles to Neuro2a cells (which will be used in our animal studies) in vitro, with and without laser irradiation (Figure 5). Our studies demonstrated that Fe_3O_4@GdPB nanoparticles exhibit marginal intrinsic toxicity (in the absence of NIR laser irradiation) to Neuro2a cells at concentrations ≥0.1 mg/mL. Neuro2a cell viability

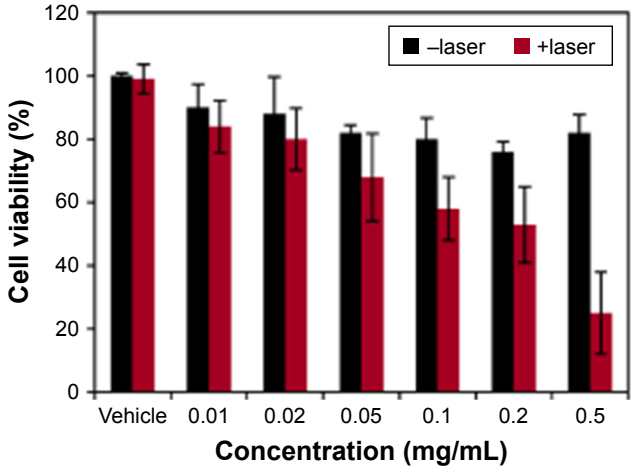

Figure 5 Intrinsic and PTT-induced cytotoxicity of varying concentrations of Fe_3O_4@GdPB nanoparticles on Neuro2a cells in vitro.
Abbreviations: Fe_3O_4@GdPB, composite iron oxide-gadolinium-containing Prussian blue; PTT, photothermal therapy.

was slightly decreased to ~80% of the vehicle-treated controls at these concentrations, suggesting that the nanoparticles can be safely used for PTT of cells without intrinsic cytotoxicity at concentrations lower than 0.1 mg/mL. Upon irradiation with the NIR laser, the Fe_3O_4@GdPB nanoparticles generated significantly increased cytotoxicity to Neuro2a cells with cell viability decreasing to <60% of controls at nanoparticle concentrations ≥0.1 mg/mL (under the experimental conditions). At a Fe_3O_4@GdPB concentration of 0.5 mg/mL, cell viability was observed to decrease 3.5-fold to around 25% upon irradiation compared to 80% viability in the absence of the laser. Together, these results establish the concentrations at which Fe_3O_4@GdPB nanoparticles do not exhibit intrinsic cytotoxicity as well as demonstrate that the nanoparticles retain their PTT properties in the presence of targeted cells.

Fe_3O_4@GdPB nanoparticles function as effective contrast agents in T1W imaging of tumors in a mouse model of neuroblastoma

As a step toward evaluating the efficacy of the Fe_3O_4@GdPB nanoparticles as effective theranostic agents in vivo, we tested the ability of the nanoparticles to function as MRI contrast agents in an animal model of neuroblastoma. Specifically, mice bearing palpable subcutaneous Neuro2a tumors (average tumor size ≥5 mm) were divided into three groups (n=5/group): 1) untreated: receiving no further treatment, 2) Fe_3O_4@GdPB-treated: tumor-bearing mice were tail-vein injected with the nanoparticles, and 3) Fe_3O_4@GdPB + magnet-treated: tumor-bearing mice were tail-vein injected with the nanoparticles and an external magnetic field was applied over the tumor for 10 minutes to direct the circulating nanoparticles into the tumor. T1W scans (Figure 6) of extracted tumor phantoms demonstrated that tumors extracted from the Fe_3O_4@GdPB + magnet-treated group exhibited increased contrast, ie, increased signal:noise ratios relative to tumors extracted from the untreated group and Fe_3O_4@GdPB-treated groups (Figure 6A). Tumors (Figure 6B) from the Fe_3O_4@GdPB + magnet-treated group exhibited an average signal:noise ratio of around 3.2, which was significantly higher ($P<0.05$) than tumors from the untreated group (~1.84) and Fe_3O_4@GdPB-treated (~2) groups. Although further T1W imaging studies in a live tumor-bearing animal are needed, these ex vivo studies demonstrate that Fe_3O_4@GdPB nanoparticles can function as effective contrast agents for T1W imaging of tumors in the presence of external magnetic guidance. Our studies represent an important first step toward achieving this important end goal of T1W resolution of tumors.

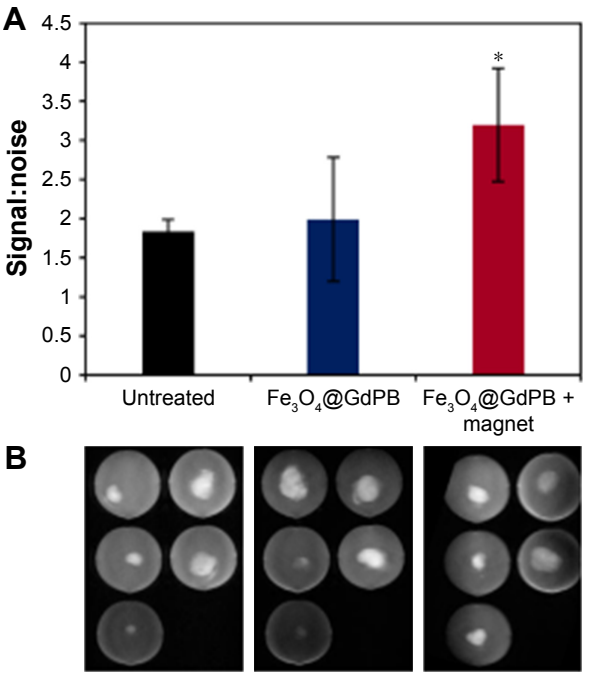

Figure 6 T1W imaging characteristics of Fe_3O_4@GdPB nanoparticles in a Neuro2a tumor model.

Notes: (**A**) Ex vivo signal:noise ratio measured in T1W images of tumors harvested from untreated, Fe_3O_4@GdPB-treated, and Fe_3O_4@GdPB + magnet-treated Neuro2a tumor-bearing mice showing significantly higher signal:noise ratio only in the presence of both the Fe_3O_4@GdPB nanoparticles plus magnet (*P-value <0.05). (**B**) Raw T1W images of tumors harvested from untreated, Fe_3O_4@GdPB-treated, and Fe_3O_4@GdPB + magnet-treated Neuro2a tumor-bearing mice.

Abbreviations: Fe_3O_4@GdPB, composite iron oxide-gadolinium-containing Prussian blue; T1W, T_1-weighted.

Fe_3O_4@GdPB nanoparticles function as effective PTT agents in a mouse model of neuroblastoma

Complementary to the T1W imaging studies, we conducted studies assessing the PTT properties of the Fe_3O_4@GdPB nanoparticles in the Neuro2a mouse model of neuroblastoma. Neuro2a tumor-bearing mice (average tumor size ≥5 mm) were divided into three groups (n=5/group): 1) untreated: receiving no further treatment, 2) Fe_3O_4@GdPB-treated: where tumor-bearing mice were tail-vein injected with the nanoparticles, and 3) Fe_3O_4@GdPB + magnet-treated: where tumor-bearing mice were tail-vein injected with the nanoparticles, and an external magnetic field was applied over the tumor for 10 minutes to direct the circulating nanoparticles into the tumor. Shortly after application of the external magnet, tumors of mice in the Fe_3O_4@GdPB-treated group and Fe_3O_4@GdPB + magnet-treated group were irradiated with the NIR laser (Figure 7). Tumor surface temperatures as measured by infrared thermometry demonstrated that mice in the Fe_3O_4@GdPB + magnet-treated group achieved an average tumor surface temperature of 52°C after 10 minutes of irradiation,

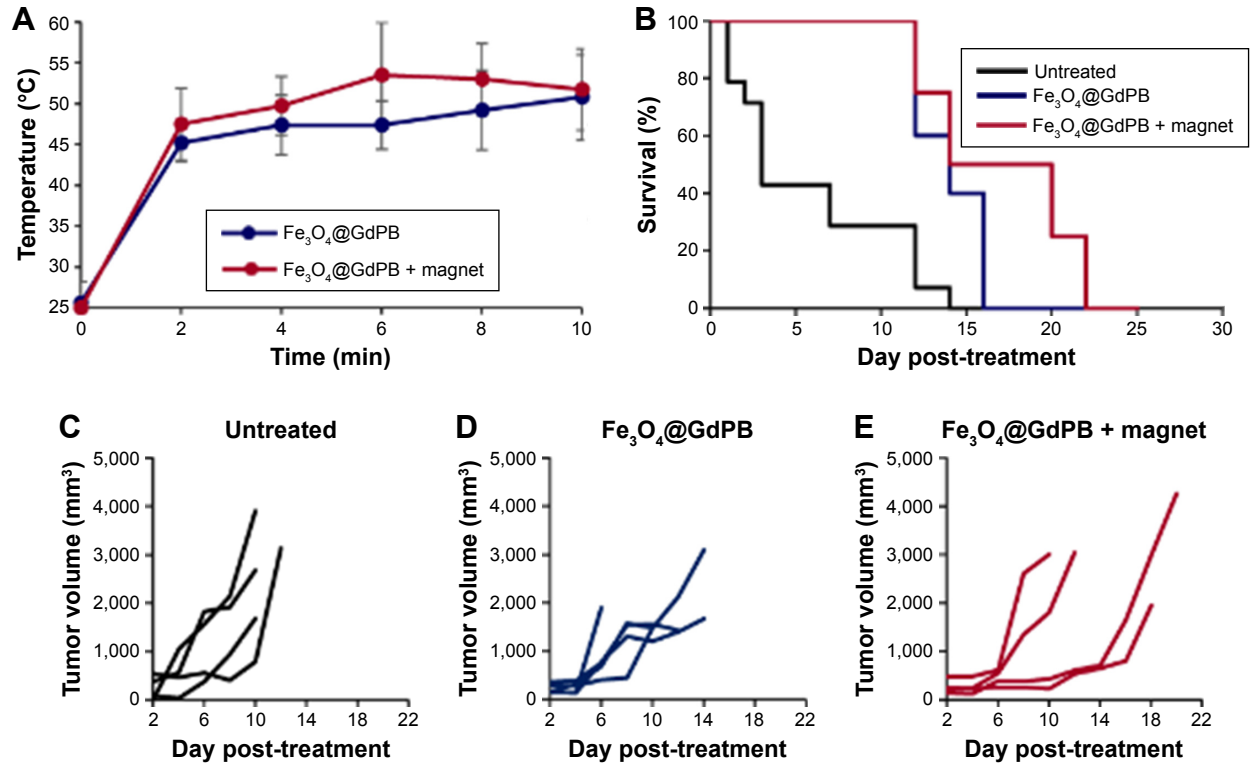

Figure 7 Photothermal therapy characteristics of Fe_3O_4@GdPB nanoparticles in a Neuro2a tumor model.
Notes: (**A**) Tumor temperatures as a function of time measured by an infrared thermal camera in Neuro2a tumor-bearing mice that are treated with either Fe_3O_4@GdPB nanoparticles or Fe_3O_4@GdPB nanoparticles + magnet. (**B**) Kaplan–Meier survival curves of Neuro2a tumor-bearing mice that are untreated, Fe_3O_4@GdPB nanoparticles + NIR laser-treated, or Fe_3O_4@GdPB nanoparticles + magnet + NIR laser-treated. (**C**–**E**) Tumor growth in Neuro2a-tumor bearing mice that are (**C**) untreated, (**D**) Fe_3O_4@GdPB nanoparticles + NIR laser-treated, and (**E**) Fe_3O_4@GdPB nanoparticles + magnet + NIR laser-treated. Each line represents a single tumor-bearing animal.
Abbreviations: Fe_3O_4@GdPB, composite iron oxide-gadolinium-containing Prussian blue; NIR, near infrared.

which was marginally higher than the tumor surface temperature of 50°C achieved in the Fe_3O_4@GdPB-treated group (Figure 7A). Furthermore, both groups achieved tumor surface temperatures that were on average >20°C above the initial tumor surface temperatures (~25°C). Our observations of significantly elevated temperatures over basal temperatures even in the Fe_3O_4@GdPB-treated group are not unexpected given that our previous studies in the same Neuro2a model have demonstrated that NIR irradiation of tumors even in the absence of PTT agents can elevate tumor surface temperatures by 5°C–10°C.[35] Additionally, when using nanoparticle-based PTT agents particularly at short time intervals after tail-vein injection (ie, <1 h), further heating is caused by nanoparticles circulating through tumor vasculature that are irradiated by the laser (intravascular heating). The addition of magnet concentrates a larger amount of nanoparticles within the tumors, which accounts for the heating observed in the Fe_3O_4@GdPB + magnet-treated group above the Fe_3O_4@GdPB-treated. Strategies that can be employed to increase the temperature elevation achieved in the Fe_3O_4@GdPB + magnet-treated group over the Fe_3O_4@GdPB-treated group are to apply the external magnet for longer periods of time, or wait until the majority of the nanoparticles are cleared from circulation (typically 1–2 hours, unless the nanoparticles are specifically designed for longer circulation times).

Kaplan–Meier survival plots demonstrated that mice in both the Fe_3O_4@GdPB-treated group and Fe_3O_4@GdPB + magnet-treated group exhibited significantly higher survival than the mice in the untreated group as determined by a log-rank test ($P<0.05$; Figure 7B). Mice in the Fe_3O_4@GdPB + magnet-treated group exhibited marginally increased survival as compared to mice in the Fe_3O_4@GdPB-treated group although this was not statistically significant. Further optimization studies with increased power, ie, increased number of mice per group, are required to completely characterize the observed PTT effects and their implications for animal survival. Finally, tumor growth curves demonstrate that PTT applied in both the Fe_3O_4@GdPB-treated and Fe_3O_4@GdPB + magnet-treated groups causes slower tumor progression as evidenced by the lower tumor growth curve slopes relative to mice in the untreated group. Once again, tumor growth in the Fe_3O_4@GdPB + magnet-treated group appeared to be marginally slower than in mice in the Fe_3O_4@GdPB-treated group but this was not

observed to be statistically significant. Taken together, our findings suggest that Fe_3O_4@GdPB nanoparticles function as effective PTT agents resulting in slower tumor growth rates and increased survival relative to untreated mice although further studies are needed to identify the optimal modes for applying the external magnet and NIR laser.

Conclusion

We have presented Fe_3O_4@GdPB nanoparticles as effective theranostic agents, particularly for T1W imaging and PTT of tumors. Our facile synthesis scheme resulted in stable Fe_3O_4@GdPB nanoparticles that exhibited composite properties of both the Fe_3O_4 and GdPB (Figures 1 and 2). The nanoparticles possessed the ability to function as effective contrast agents in both T1W and T2W scans (Figure 3) as well as effective PTT agents (Figure 4). The Fe_3O_4@GdPB nanoparticles generated cytotoxicity of targeted Neuro2a cells upon laser irradiation in vitro (Figure 5). Ex vivo imaging studies demonstrated that the nanoparticles increased signal:noise ratios in T1W scans of tumor phantoms relative to controls (Figure 6). Finally, the nanoparticles functioned as effective PTT agents in vivo by decreasing tumor growth rate and increasing survival relative to untreated controls (Figure 7). Our findings demonstrate the theranostic utility of our Fe_3O_4@GdPB nanoparticles and represent an important prelude to their eventual preclinical to clinical translation in treating cancer.

Acknowledgments

This work was supported by a Research Advisory Council award from the Sheikh Zayed Institute for Pediatric Surgical Innovation and a Pilot Studies Award from the Joseph E Robert Jr. Endowment Awards at Children's National Health System, and funding was provided by MedImmune.

Author contributions

All authors contributed toward data analysis, drafting and critically revising the paper and agree to be accountable for all aspects of the work.

Disclosure

The authors report no conflicts of interest in this work.

References

1. Pene F, Courtine E, Cariou A, Mira JP. Toward theragnostics. *Crit Care Med*. 2009;37(1 suppl):S50–S58.
2. Jorgensen JT, Hersom M. Companion diagnostics-a tool to improve pharmacotherapy. *Ann Transl Med*. 2016;4(24):482.
3. Janib SM, Moses AS, MacKay JA. Imaging and drug delivery using theranostic nanoparticles. *Adv Drug Deliv Rev*. 2010;62(11):1052–1063.
4. Xie J, Lee S, Chen X. Nanoparticle-based theranostic agents. *Adv Drug Deliv Rev*. 2010;62(11):1064–1079.
5. Kievit FM, Zhang M. Surface engineering of iron oxide nanoparticles for targeted cancer therapy. *Acc Chem Res*. 2011;44(10):853–862.
6. Kievit FM, Zhang M. Cancer nanotheranostics: improving imaging and therapy by targeted delivery across biological barriers. *Adv Mater*. 2011;23(36):H217–H247.
7. Moon HK, Lee SH, Choi HC. In vivo near-infrared mediated tumor destruction by photothermal effect of carbon nanotubes. *ACS Nano*. 2009;3(11):3707–3713.
8. Tan A, Yildirimer L, Rajadas J, De La Pena H, Pastorin G, Seifalian A. Quantum dots and carbon nanotubes in oncology: a review on emerging theranostic applications in nanomedicine. *Nanomedicine (Lond)*. 2011;6(6):1101–1114.
9. Dickerson EB, Dreaden EC, Huang X, et al. Gold nanorod assisted near-infrared plasmonic photothermal therapy (PPTT) of squamous cell carcinoma in mice. *Cancer Lett*. 2008;269(1):57–66.
10. Gormley AJ, Larson N, Sadekar S, Robinson R, Ray A, Ghandehari H. Guided delivery of polymer therapeutics using plasmonic photothermal therapy. *Nano Today*. 2012;7(3):158–167.
11. Gillies ER, Frechet JM. Dendrimers and dendritic polymers in drug delivery. *Drug Discov Today*. 2005;10(1):35–43.
12. Li X, Takashima M, Yuba E, Harada A, Kono K. PEGylated PAMAM dendrimer-doxorubicin conjugate-hybridized gold nanorod for combined photothermal-chemotherapy. *Biomaterials*. 2014;35(24):6576–6584.
13. Liu Q, Zhu H, Qin J, Dong H, Du J. Theranostic vesicles based on bovine serum albumin and poly(ethylene glycol)-block-poly(L-lactic-co-glycolic acid) for magnetic resonance imaging and anticancer drug delivery. *Biomacromolecules*. 2014;15(5):1586–1592.
14. Song J, Pu L, Zhou J, Duan B, Duan H. Biodegradable theranostic plasmonic vesicles of amphiphilic gold nanorods. *ACS Nano*. 2013;7(11):9947–9960.
15. Schutz CA, Juillerat-Jeanneret L, Mueller H, Lynch I, Riediker M; NanoImpactNet Consortium. Therapeutic nanoparticles in clinics and under clinical evaluation. *Nanomedicine (Lond)*. 2013;8(3):449–467.
16. Anselmo AC, Mitragotri S. Nanoparticles in the clinic. *Bioeng Transl Med*. 2016;1(1):10–29.
17. Qiao R, Yang C, Gao M. Superparamagnetic iron oxide nanoparticles: from preparations to in vivo MRI applications. *J Mater Chem*. 2009;19:6274–6293.
18. Faustino PJ, Yang Y, Progar JJ, et al. Quantitative determination of cesium binding to ferric hexacyanoferrate: Prussian blue. *J Pharm Biomed Anal*. 2008;47(1):114–125.
19. FDA. *Radiogardase – Ferric Hexacyanoferrate(ii) Capsule*. 2016. Available from: http://www.accessdata.fda.gov/drugsatfda_docs/label/2008/021626s007lbl.pdf. Accessed June 3, 2016.
20. Yang Y, Faustino PJ, Progar JJ, et al. Quantitative determination of thallium binding to ferric hexacyanoferrate: Prussian blue. *Int J Pharm*. 2008;353(1–2):187–194.
21. Pintaske J, Martirosian P, Graf H, et al. Relaxivity of gadopentetate dimeglumine (magnevist), gadobutrol (gadovist), and gadobenate dimeglumine (MultiHance) in human blood plasma at 0.2, 1.5, and 3 Tesla. *Invest Radiol*. 2006;41(3):213–221.
22. Rohrer M, Bauer H, Mintorovitch J, Requardt M, Weinmann HJ. Comparison of magnetic properties of MRI contrast media solutions at different magnetic field strengths. *Invest Radiol*. 2005;40(11):715–724.
23. Fu G, Liu W, Li Y, et al. Magnetic Prussian blue nanoparticles for targeted photothermal therapy under magnetic resonance imaging guidance. *Bioconjug Chem*. 2014;25(9):1655–1663.
24. Xue P, Bao J, Wu Y, Zhang Y, Kang Y. Magnetic Prussian blue nanoparticles for combined enzyme-responsive drug release and photothermal therapy. *RSC Adv*. 2015;5:28401–28409.
25. Xue P, Bao J, Zhang L, et al. Functional magnetic Prussian blue nanoparticles for enhanced gene transfection and photothermal ablation of tumor cells. *J Mater Chem B*. 2016;4:4717–4725.
26. Na HB, Hyeon T. Nanostructured T1 MRI contrast agents. *J Mater Chem*. 2009;19:6267–6273.

27. Chakrabarti L, Morgan C, Sandler AD. Combination of Id2 knockdown whole tumor cells and checkpoint blockade: a potent vaccine strategy in a mouse neuroblastoma model. *PLoS One*. 2015;10(6):e0129237.
28. Williams EL, Dunn SN, James S, et al. Immunomodulatory monoclonal antibodies combined with peptide vaccination provide potent immunotherapy in an aggressive murine neuroblastoma model. *Clin Cancer Res*. 2013;19(13):3545–3555.
29. Siegel RL, Miller KD, Jemal A. Cancer statistics, 2016. *CA Cancer J Clin*. 2016;66(1):7–30.
30. Ward E, Desantis C, Robbins A, Kohler B, Jemal A. Childhood and adolescent cancer statistics, 2014. *CA Cancer J Clin*. 2014;64(2):83–103.
31. Fernandes R, Tsao CY, Hashimoto Y, et al. Magnetic nanofactories: localized synthesis and delivery of quorum-sensing signaling molecule autoinducer-2 to bacterial cell surfaces. *Metab Eng*. 2007;9(2):228–239.
32. Dumont MF, Hoffman HA, Yoon PR, et al. Biofunctionalized gadolinium-containing Prussian blue nanoparticles as multimodal molecular imaging agents. *Bioconjug Chem*. 2014;25(1):129–137.
33. Vojtech JM, Cano-Mejia J, Dumont MF, Sze RW, Fernandes R. Biofunctionalized Prussian blue nanoparticles for multimodal molecular imaging applications. *J Vis Exp*. 2015;(98):e52621.
34. Dumont MF, Yadavilli S, Sze RW, Nazarian J, Fernandes R. Manganese-containing Prussian blue nanoparticles for imaging of pediatric brain tumors. *Int J Nanomedicine*. 2014;9:2581–2595.
35. Hoffman HA, Chakarbarti L, Dumont MF, Sandler AD, Fernandes R. Prussian blue nanoparticles for laser-induced photothermal therapy of tumors. *RSC Adv*. 2014;4(56):29729–29734.
36. Roper DK, Ahn W, Hoepfner M. Microscale heat transfer transduced by surface plasmon resonant gold nanoparticles. *J Phys Chem C Nanomater Interfaces*. 2007;111(9):3636–3641.
37. Cano-Mejia J, Burga RA, Sweeney EE, et al. Prussian blue nanoparticle-based photothermal therapy combined with checkpoint inhibition for photothermal immunotherapy of neuroblastoma. *Nanomedicine*. 2017;13(2):771–781.
38. Shokouhimehr M, Soehnlen ES, Hao J, et al. Dual purpose Prussian blue nanoparticles for cellular imaging and drug delivery: a new generation of T1-weighted MRI contrast and small molecule delivery agents. *J Mater Chem*. 2010;20:5251–5259.
39. Shokouhimehr M, Soehnlen ES, Khitrin A, Basu S, Huang SD. Biocompatible Prussian blue nanoparticles: preparation, stability, cytotoxicity, and potential use as an MRI contrast agent. *Inorg Chem Commun*. 2010;13:58–61.

Supplementary material

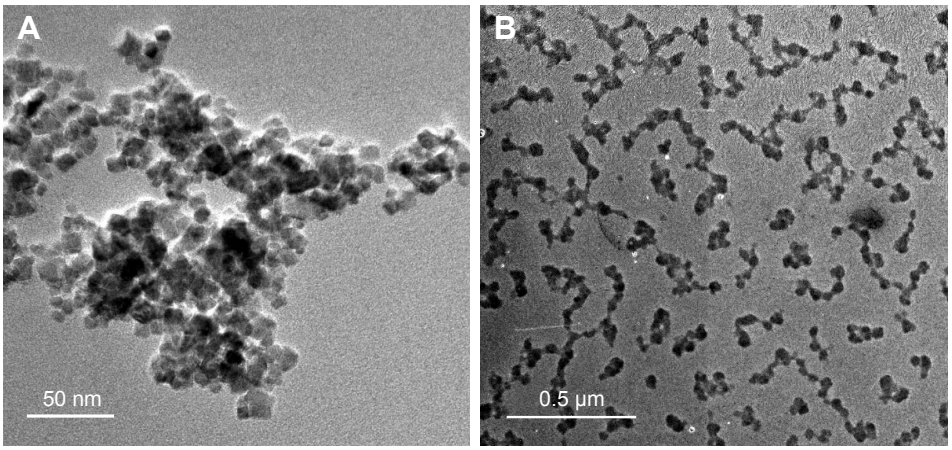

Figure S1 Representative TEM images of (**A**) Fe_3O_4 and (**B**) Fe_3O_4@GdPB nanoparticles as synthesized.
Note: The nanoparticles size analysis was performed using ImageJ by manually measuring the size of the individual nanoparticles from the TEM images, which yielded a mean particle diameter of 8.0±2.2 nm for Fe_3O_4 and 28.2±8.3 nm for Fe_3O_4@GdPB.
Abbreviations: Fe_3O_4@GdPB, composite iron oxide-gadolinium-containing Prussian blue; TEM, transmission electron microscopy.